© S. Hirzel Verlag · EAA
acta acustica · ACUSTICA
Vol. 87 (2001) 738 – 747

Relative-Time Inversions in the Labrador Sea Acoustic Tomography Experiment

D. Kindler, U. Send
Institut für Meereskunde an der Universität Kiel, Düsternbrooker Weg 20, D-24105 Kiel, Germany

E. K. Skarsoulis
Institute of Applied and Computational Mathematics, Foundation for Research and Technology Hellas, P.O. Box 1527, 711 10 Heraklion, Crete, Greece

Summary
One-year long travel-time data from the second deployment period of the Labrador Sea acoustic tomography experiment are analyzed, using a relative-time matched-peak approach, in order to invert for the sound-speed field and simultaneously solve for an unknown travel-time offset. From the relative-time inversions oceanographic information in terms of vertically averaged temperatures are deduced, yielding satisfactory matching with respect to available independent observations. The estimated offsets can be attributed to differential clock drifts, showing a clear parabolic behaviour over the course of the experiment, reaching maximum deviations from linear clock drift corrections (end-point calibrations) of the order of 50 ms. By applying the estimated second-order corrections to the travel-time data, absolute-time matched-peak inversions can then be performed. The used matched-peak approach accounts for the non-linear behaviour of travel times, which is due to the seasonally variable acoustic propagation conditions in the probed region, and turns out to be an appropriate tool in dealing with unknown travel-time offsets.

PACS no. 43.30.Pc, 43.30.Qd, 43.60.Pt, 43.60.Rw

1. Introduction

A multi-year ocean acoustic tomography experiment was initiated in summer 1996 in the central Labrador Sea [1]. This experiment is part of an ongoing research project at the Institute of Marine Science of Kiel addressing the dynamics and the variability of the thermohaline circulation in the North Atlantic Ocean [1]. In the Labrador Sea there is high potential for deep mixing in winter, and hence for annual deep water replenishment reaching down to more than 2000 m during cold winters. This deep water renewal path is believed to be one of the important downward connections between the northward flowing upper and the southward flowing lower branch of the North Atlantic overturning circulation. Hence, the Labrador Sea is expected to be a key area for this thermal and haline driven overturning, and thus for the formation of the North Atlantic deep water.

The purpose of acoustic measurements in this context is to study the large-scale effects of winter cooling, deep mixing by convection and subsequent warming and restratification on the meso-scale. The first tomographic array in the central Labrador Sea was installed in August 1996 and redeployed in the summers of 1997, 1998, 1999 and 2000 in order to measure acoustic travel times over distances of 140-250 km. By inverting the travel times of different ray paths between the transmitters and receivers into sound speed and hence into temperature, time series of horizontally and vertically integrated properties like ocean heat content can be produced [2].

Usually in the course of such experiments, the timekeeping and instrument navigation is good enough (after possibly some initial offsets that are applied) to allow usage of the absolute travel times of all the arrivals that are observed in a reception. In some cases, however, or in some types of approaches, each reception has an unknown offset due to e.g. drifting transmitters/receivers, insufficient navigation of the instruments on a mooring, or uncertain clock offsets. In such cases, only the relative travel-time differences between different arrivals (different ray paths) can be used, since the absolute arrival time has an arbitrary offset in each reception. In the case of the Labrador Sea experiment, the use of relative travel times was motivated by suspected problems with the timekeeping (clock drift stability).

To measure travel times with accuracy of a few milliseconds, required for absolute-time inversions, extremely stable clocks are required. Given the current state of the art, the energy requirements for one-year autonomous operation of the tomographic transceiver systems can only be met by crystal-driven clocks, which however have a limited accuracy. In the deployment and recovery phases of the experiment the offset (i.e. the integrated drift) of the clocks can be determined; such an end-point calibration is applied relative to the highly accurate GPS satellite time. Nevertheless, this procedure can only compensate for the linear component of the clock drift. It is known from previous experiments [3] that clocks of the particular type exhibit a significant second-order drift component, which has to be corrected for.

A relative-time inversion procedure is presented here for the estimation of the clock drift, simultaneously with the oceanographic inversions, provided that the travel-time data have been corrected for the mooring distance and mooring motion. The basic idea is to use relative-time inversions by considering the observed travel times in each reception fixed

Received 6 June 2001,
accepted 18 October 2001.

up to an unknown time shift, which is attributed to the differential clock drift between emitting and receiving instrument.

A variety of different inversion methods can be found in the literature for the analysis of travel-time data, from conventional linear inversions of identified peak tracks [4], [5] to automatic non-linear inversions with simultaneous identification of (unidentified) travel-time data [6], [7], [8]. The travel-time behaviour in the Labrador Sea is non-linear; this is due to the passage from surface-reflected propagation conditions in winter to refracted propagation in summer, as described in Section 2. In this connection, the matched-peak inversion approach [8] is adopted.

The matched-peak approach allows for automatic non-linear inversion of unidentified travel-time data by-passing the explicit solution of the tracking and identification problem. Using the linearized model relations about a set of background states arrival times and associated errors are calculated on a fine grid of model states discretizing the sound-speed parameter space. Each model state can explain a number of observed peaks in a reception lying within the uncertainty intervals of the corresponding predicted arrival times. The model states that identify the maximum number of observed peaks, described in terms of mean values and variances, provide a statistical answer (matched-peak solution) to the inversion problem. Each reception can be treated independently, i.e. no constraints are posed from previous-reception identification or inversion results. Accordingly, there is no need for initialization of the inversion procedure and, furthermore, discontinuous travel-time data can be treated.

The contents of the work are organized as follows: A general description of the ocean acoustic tomography experiment in the Labrador Sea is given in section 2 together with an overview of the deployment period and the insonified sections treated in this paper. Section 3 addresses the modelling of arrival times and the matched-peak approach for relative-time inversion. In section 4 one-year long travel-time data from the second year (August 1997- July 1998) of the Labrador Sea experiment are analyzed and differential clock drifts are estimated. The obtained results are compared with data from independent measurements. The discussion of the results follows in the last section together with some concluding remarks.

2. Experiment description

The ongoing Labrador Sea Tomography Experiment was initiated in August 1996. It consists of an array of 3 or 4 moored tomographic instruments, depending on year, which are redeployed annually in late spring or summer. In this paper we concentrate on data from the second deployment period which lasted from August 1997 until July 1998. The acoustic array for this period is shown in Figure 1. It consisted of three Webb-type transceivers located at the mooring positions K12, K14 and K17, and one HLF5-type transceiver at K11. The choice of the positions is based on some a priori knowledge about the location of open ocean convection events in the central to southwestern Labrador Sea in late winter [9], such

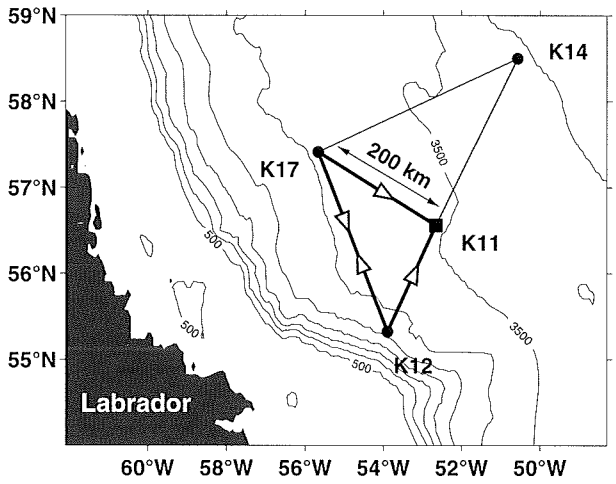

Figure 1. Geometry of Labrador Sea acoustic tomography mooring array during Aug. 1997 – Jul. 1998. Solid dots mark positions of 400 Hz Webb-type transceivers, solid square marks HLF5-type transceiver. Arrows indicate direction of transmissions along treated sections, highlighted by heavy lines. Contour interval for isobaths is 500 m.

Table I. Experiment geometry.

		K11	K12	K17
distance (km)	K11	-	157.6	205.7
travel time (s)	K11	-	106.5	139.4
distance (km)	K12	-	-	257.3
travel time (s)	K12	-	-	174.3
distance (km)	K17	-	257.3	-
travel time (s)	K17	-	174.3	-
depl. depth (m)		128	131	134
water depth (m)		3490	2380	2965

that the connection lines would cover, at least partially, the expected region of deep mixing.

An optimal deployment depth for all instruments, in terms of the maximum amount of sound-speed information to be recovered, was chosen to equal 150 m, nominally. Typical distances between mooring pairs (with good data in terms of signal-to-noise-ratio) ranged between 150 km and 330 km (see Table I for individual distances and actual deployment depths). The Webb-type sources transmitted for either 80 or 150 seconds 6 times a day over one year at a central frequency of 400 Hz with an effective bandwidth of 100 Hz. The HLF5 source (with 250 Hz central frequency) never transmitted due to a failure in the power supply. Nevertheless, the receiver of this instrument was able to receive all the other instruments. Hence, there were reciprocal (two-way) transmission for the instrument pairs K12-K17 and K14-K17, whereas the other pairs yielded one-way data only.

The transmissions consisted alternatingly of 16 or 30 phase shift keying (PSK) sequences, each sequence lasting for 5.11 seconds. At the receiving instrument 14 or 28 repetitions of such sequences were recorded, respectively. After each reception the signals were demodulated and the longer re-

ceptions (28 repetitions) were coherently averaged in-situ, before being stored on a hard disk. After recovery of the instruments the recorded receptions were matched-filtered, i.e. correlated with a replica of the emitted PSK signal [10]. The amplitude of the result, called arrival pattern, is equivalent to the pressure amplitude that would be recorded at the receiver in the time domain if the source emitted a pulsed signal whose shape in the time domain is identical with the autocorrelation of the PSK signal. The advantage of using PSK signals is that the signal energy is spread over a long time period, such that the power levels required are dramatically reduced. A sample arrival pattern is shown in Figure 7 to be discussed later. About 12 well identifiable arrival peaks (grouped in 4 triplets) can be detected there, corresponding to acoustic eigenrays with lower turning depths between about 600 m (later arrivals) and 2100 m (earlier arrivals).

In order to correct the recorded travel times for mooring motion (which has a significant impact in the Labrador Sea) the exact positions (to within a few meters) of each instrument had to be determined before and after each transmission or reception. This was done by an acoustic underwater positioning system which consisted of a 10 kHz pinger at the transceiver and an array of three bottom mounted acoustic transponders (pinging at 11.5, 12.0 and 12.5 kHz, respectively) deployed in a triangular shape around the base of each mooring.

To invert acoustic travel times into sound speed and hence into temperature (having the largest influence on sound speed) a certain amount of a priori knowledge about the typical sound-speed variability of the probed region is required. The common assumption, that the observed travel-time fluctuations can largely be explained by the horizontally averaged field, reduces the sought sound-speed field from a 2-D section to a one-dimensional vertical profile. Thus, the variability is sufficiently described by a set of vertical sound-speed modes, which in our case were calculated by an EOF analysis applied to all available CTD profiles collected during the different Labrador Sea cruises in 1990s. In Figure 2 the first 5 empirical orthogonal functions (EOFs) from this analysis, together with the used basic reference sound-speed profile are shown. The rms values of the EOF amplitudes are 17.7, 5.8, 3.9, 2.1 and 1.8 ms^{-1}. The first EOF is strongly intensified towards the surface in the upper 100 m, representing the bulk of the near-surface seasonal variability, reflected by the large rms value. With increasing order the rms value decreases and the excitation of the EOF extends to larger depth.

The acoustic travel-time data analyzed in the following sections come from the sections K11-K12, K11-K17 and K12-K17, defining the southern triangle in Figure 1. The deployment depths, the typical distances and travel times and the typical water depths for these sections are given in Table I. The predicted travel times along the section K11-K12 corresponding to variations of the mean reference sound-speed profile in the direction of the first EOF (spanning the typical range of near-surface variability) are shown in Figure 3. The predictions were made using a *raytrace* ocean sound propagation model. The calculation yielded arrival peaks from

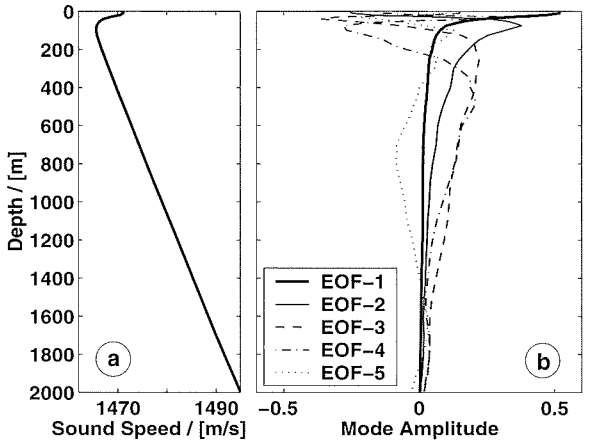

Figure 2. (a) Basic reference sound-speed profile, and (b) the five most significant empirical orthogonal functions (EOFs) in the Labrador Sea.

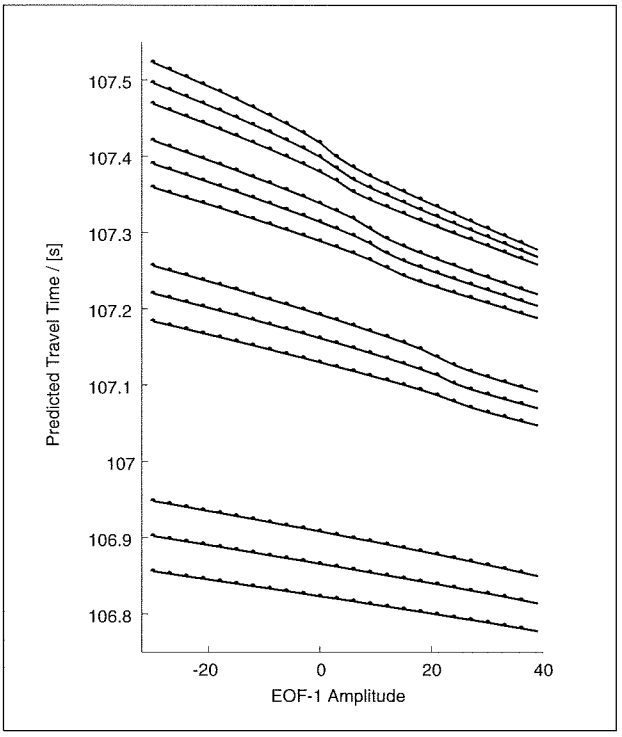

Figure 3. Predicted ray arrival times as a function of EOF-1 amplitude over a typical variability range.

deeper rays (first triplet) to shallower rays (last triplet) having lower turning depths between 2100 m and 600 m, respectively.

A non-linear character is evident in Figure 3; in particular, transition regions can be seen, different for different peaks, where the non-linearity is stronger. These intervals correspond to the passage from surface-reflected propagation (typical for winter conditions / lower EOF-1 amplitudes) to refracted propagation (typical for summer conditions / higher EOF-1 amplitudes). The transition takes place when the sound speed at the surface equals the sound speed at the

lower turning depth of the ray. The latter is larger for deeper rays – corresponding to early arrivals – than for shallower rays – corresponding to later arrivals. Accordingly, the transition will take place at larger EOF-1 amplitudes for early arrivals than for later ones; this behaviour is seen in Figure 3. The transition of the first group of arrivals (earliest triplet in Figure 3) takes place at values larger than 40; implying that this group always corresponds to surface-reflected propagation in the considered variability range and thus exhibits a linear behaviour with respect to the amplitude of EOF-1.

An approach for the solution of the travel-time inversion problem taking into account the above non-linear behaviour of travel times is described in the following section.

3. Inversion approach

An inversion method is presented in this section, based on the matched-peak approach, for obtaining sound-speed estimates from measured relative travel-time differences, i.e. from travel times fixed up to an unknown time shift. The matched-peak approach by-passes the explicit solution of the peak identification problem (association between model and observed travel times) and also accounts for the non-linear behaviour of travel times.

Using the mean profile and the sound-speed modes shown in Figure 2, and assuming a range-independent ocean environment the sound-speed variability in the area of interest can be represented through a modal expansion

$$c(z) = c_0(z) + \sum_{l=1}^{L} \vartheta_l f_l(z), \tag{1}$$

where $c_0(z)$ and $f_l(z), l = 1, \ldots, L$, denote the mean profile and the empirical orthogonal functions, respectively.

3.1. Model relations

The functional dependence of the arrival times τ_i, $i = 1, 2, \ldots, I$, for a particular source-receiver pair, on the sound speed can be written as a parametric dependence, non-linear in general,

$$\tau_i = g_i(\boldsymbol{\vartheta}), \quad i = 1, 2, \ldots, I, \ \boldsymbol{\vartheta} \in \Theta, \tag{2}$$

where $\boldsymbol{\vartheta} = (\vartheta_1, \ldots, \vartheta_L)'$ is the modal parameter vector and Θ is the parameter space spanning the anticipated sound-speed variability. Figure 3 shows the dependence of ray arrival times on ϑ_1, the amplitude of the most significant mode. Although this dependence is non-linear, in the case of small perturbations about a background state $\boldsymbol{\vartheta}^{(b)}$ it can be linearized

$$\boldsymbol{\tau}(\boldsymbol{\vartheta}) = \boldsymbol{\tau}^{(b)} + \boldsymbol{G}^{(b)}(\boldsymbol{\vartheta} - \boldsymbol{\vartheta}^{(b)}), \tag{3}$$

where $\boldsymbol{\tau} = (\tau_1, \ldots, \tau_I)'$ is the arrival-time vector and $\boldsymbol{\tau}^{(b)} = \boldsymbol{\tau}(\boldsymbol{\vartheta}^{(b)})$ denotes the background arrival times. $\boldsymbol{G}^{(b)}$ is the observation (influence) matrix corresponding to the background state $\boldsymbol{\vartheta}^{(b)}$ and relating the sound-speed and travel-time variability, $G_{il}^{(b)} = \partial g_i(\boldsymbol{\vartheta}^{(b)})/\partial \vartheta_l$.

In the case of non-linear model relations eq. (3) can be extended to cover the whole range of variability by considering a set of background states, rather than a single one; the linearized model relation can then be used with respect to the closest background state each time. In this connection, the index b is considered in the following as a variable, $b \in \mathcal{B}$, from the set $\mathcal{B}$ of discrete background states. In this way the non-linear model relation (2) is replaced by a set of linearized ones.

Besides the sound-speed changes there are also other factors that affect travel times, such as mooring motions, differences between theoretical and actual distances between moorings, drifts of instrument clocks as well as internal instrument delays. These factors must be corrected or accounted for when performing inversions. While clock drifts and internal delays cause translation of arrival times by a constant offset in each reception, a change in range between source and receiver – due to unknown mooring motion or position – has in general both a translation and a stretching/shrinking effect on the arrival times [11], [12]. Nevertheless, in the case of small changes in range the stretching/shrinking effect is small and can be neglected. By considering such cases and including all the possible offset factors in a single variable denoted by δt the observed travel times $\boldsymbol{\tau}^{(o)}$ can be written in the form

$$\boldsymbol{\tau}^{(o)} = \boldsymbol{\tau}^{(b)} + \boldsymbol{G}^{(b)}(\boldsymbol{\vartheta} - \boldsymbol{\vartheta}^{(b)}) + \boldsymbol{u}\delta t + \boldsymbol{\nu}. \tag{4}$$

The vector $\boldsymbol{u}$ in (4) is a unity vector, with all its elements equal 1 (implying that the value of δt is the same for all arrival times in the same reception), and the vector $\boldsymbol{\nu}$ in (4) accounts for the cumulative modelling and observation error.

3.2. Matched-peak relative-time inversion

In the matched-peak approach [8] the parameter space Θ is discretized into a regular grid, with discretization steps $\delta\boldsymbol{\vartheta}$, which is superposed on the grid of background states. Using the linearized model relations, arrival-time predictions are made for each discrete model state $\tilde{\boldsymbol{\vartheta}}$ (a tilde denotes quantities referring to the discretization grid), depending also on the bias δt

$$\tilde{\boldsymbol{\tau}}(\tilde{\boldsymbol{\vartheta}}; \delta t) = \boldsymbol{\tau}^{(b)} + \boldsymbol{G}^{(b)}(\tilde{\boldsymbol{\vartheta}} - \boldsymbol{\vartheta}^{(b)}) + \boldsymbol{u}\delta t. \tag{5}$$

Each discrete model state refers to a particular background state (the one that lies closest). An estimate for the upper-bound of the prediction error is given by the sum of the observation/modelling error $\boldsymbol{\nu}$ and a discretization error, which depends on the background state and the discretization steps

$$e(b, \delta\boldsymbol{\vartheta}) = \frac{1}{2}\left|\boldsymbol{G}^{(b)}\right| \delta\boldsymbol{\vartheta} + \boldsymbol{\nu}, \tag{6}$$

where $|\boldsymbol{G}^{(b)}|$ denotes the matrix whose elements are the absolute values of the elements of $\boldsymbol{G}^{(b)}$. Each of the predicted arrival times (5) is allowed to associate with observed arrival

acta acustica · ACUSTICA
Vol. 87 (2001)

times if their time difference is smaller than the corresponding travel-time error (6). A matching index M can be thus calculated, denoting the number of identifiable peaks, i.e. the number of peaks in the measured arrival pattern that can be associated with the predicted arrival times $\tilde{\tau}(\tilde{\vartheta}; \delta t)$, for each $\tilde{\vartheta}$ and each value of δt

$$M = M(\tilde{\vartheta}; \delta t). \tag{7}$$

M can be calculated in a straightforward and simple way. The associated computational burden is much smaller than for building up the set of all possible trial identifications (possible associations between predicted and observed peaks), which is necessary e.g. for explicitly solving the identification problem [7].

According to the peak-matching principle, the sound-speed parameters and the travel-time bias can be estimated by finding the population of discrete model states $\tilde{\vartheta}$ and corresponding travel-time offsets δt that maximize the number of peak identifications in a particular reception

$$V = \left\{ (\tilde{\vartheta}; \delta t) : \; M(\tilde{\vartheta}; \delta t) = \max \right\}. \tag{8}$$

In the above optimization the search with respect to the travel-time offset δt has to be carried out with sufficient resolution of a few milliseconds.

An alternative to avoid the search over δt, and thus accelerate the maximization procedure, is to associate a specific δt value with each discrete model state. This can be done by adjusting the arrival time of a reference peak (e.g. the first clear arrival) in the prediction and the data. This leads to an offset

$$\delta \hat{t}(\tilde{\vartheta}) = \tau_{ref}^{(o)} - \tilde{\tau}_{ref}(\tilde{\vartheta}; 0), \tag{9}$$

where $\tilde{\tau}_{ref}$ and $\tau_{ref}^{(o)}$ is the predicted (from (5)) and observed arrival time of the reference peak, respectively, in the particular reception. Using this time offset, the predicted and measured arrival time of the reference peak coincide

$$\tilde{\tau}_{ref}(\tilde{\vartheta}; \delta \hat{t}(\tilde{\vartheta})) = \tau_{ref}^{(o)}. \tag{10}$$

The corresponding matching index, denoted by $\hat{M}$, is given by

$$\hat{M}(\tilde{\vartheta}) = M(\tilde{\vartheta}; \delta \hat{t}(\tilde{\vartheta})). \tag{11}$$

Accordingly, each discrete model state $\tilde{\vartheta}$ is associated with a certain time offset $\delta \hat{t}(\tilde{\vartheta})$ and matching index $\hat{M}(\tilde{\vartheta})$. The relative-time matched-peak solution consists in this case in maximizing $\hat{M}$ with respect to $\tilde{\vartheta}$, i.e. finding the population of model states that explain the maximum number of observed peaks, after having adjusted the reference arrival times. This variation of the relative-time matched-peak approach is used for the data analysis below. It requires the tracking and identification of the reference peak. i.e. of a single peak, in the data, whereas it by-passes the tracking and identification problem for the remaining peaks.

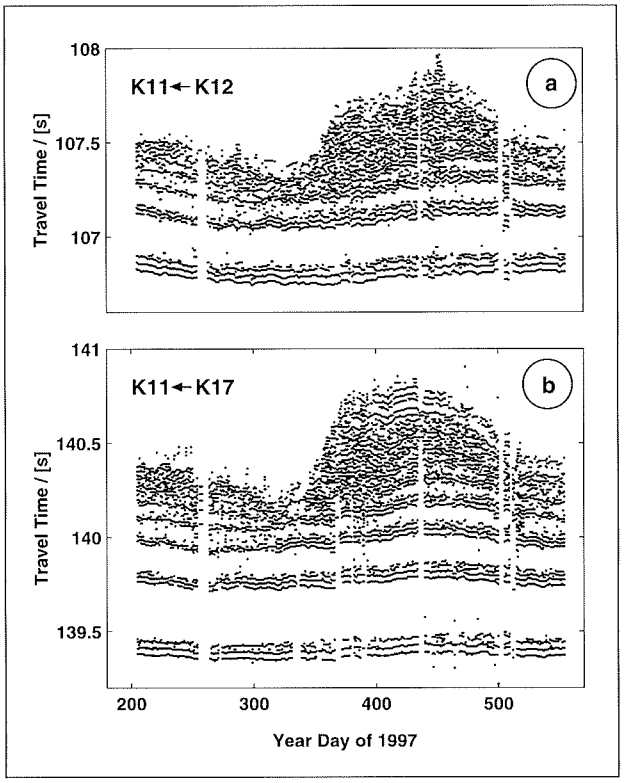

Figure 4. Measured acoustic arrival times at K11 from (a) K12 and (b) K17, vs. experiment time (yeardays 1997) spanning the period from August 1997 to July 1998.

The data treated in the following section have been corrected for the difference between theoretical and actual source-receiver range and internal instrument delays, as well as for mooring motion and linear clock drift (end-point calibration), prior to the inversions. Accordingly the estimated time offsets can be attributed to deviations of the differential clock drift from linearity.

4. Data analysis

In this section one-year long travel-time data from the second year (August 1997-July 1998) of the Labrador Sea Experiment are analyzed. The main focus is on the section K11-K12 (see Figure 1). The tomography data are presented first followed by the results from the relative-time inversion approach, i.e oceanographic inversions along with the simultaneous estimates for the differential clock drift. In the end of this section absolute-time inversion results for the section K11-K12 are presented, based on corrected travel-time data using the estimated second-order clock drifts.

4.1. Data description

The upper panel of Figure 4 shows the acoustic arrival times at K11 from K12 during one year, from August 1997 to July 1998. The horizontal axis represents yeardays of 1997, whereas the vertical axis measures arrival time in seconds.

In the lower panel of Figure 4 the acoustic data from the section K11-K17 are shown for comparison. These data have resulted from correlation processing of the raw tomography data and after the application of mooring-motion correction, calibration for mean mooring position, and linear clock drift (end-point) calibration. Furthermore, a 3-day sliding average has been applied keeping a one-day sampling, i.e. for each calendar day the arrival patterns measured from the preceding to the following day have been incoherently averaged, provided that they are of good quality (in terms of SNR).

To obtain the most significant peaks the arrival patterns were normalized with respect to the noise rms level. Then, that part of the signal lying higher than 2-3 times the rms noise level was considered as useful signal, from which the 50 most significant relative maxima (in terms of SNR) were taken and used for the further processing.

The gaps with no data to be seen for both sections (more pronounced along K11-K17) are due to excessive noise caused by strong oceanic currents. Besides the noise such events also cause the mooring lines to lean substantially pulling the instruments down to depths sometimes several hundreds of meters below their nominal deployment depth. To separate between usable receptions and poor-quality data, a signal-to-noise ratio of 25 dB was used. A large seasonal variation can be seen in Figure 4. Higher temperatures in autumn (centered at yearday 300) cause a sound-speed increase which in turn gives rise to shorter travel times, whereas lower temperatures in late winter (around yeardays 450 to 500) cause a sound-speed decrease and they are thus associated with longer travel times.

Three to four arrival groups can be distinguished in the receptions along K11-K12 for most of the experiment duration (four to five groups along K11-K17). These groups can be associated with particular ray groups corresponding to steep launch angles and lower turning depths between 600 and 2100 m, as mentioned in the Section 2. The later part of the receptions is difficult to be treated in a ray-theoretic context [13] and even though its variability is large it is not used here. For the analysis of section K11-K12 4 groups (triplets) of early ray arrivals are used. For K11-K17 and K12-K17 4 and 5 groups are considered, respectively. For the following inversions a set of background states is defined as EOF-1 variations of the basic reference profile over the ϑ_1-interval [-30,+60], covering 2-3 standard deviations of the corresponding amplitude, with a ϑ_1-step of 3. The arrival times and observation matrix $\boldsymbol{G}^{(b)}$ at each background state is calculated using a ray-theoretic code.

A time-variable parameter domain (search interval) is considered for ϑ_1, $\pm$ 9 about the historical mean value of ϑ_1 for each day of the year. The restriction of the parameter domain for ϑ_1 significantly reduces the computational burden, by avoiding calculations for unnatural model states which lie outside the anticipated variability range for each season. Note that the reduction of the computational burden is necessary, since the identification and inversion problem is non-linear in this case. For the remaining four EOFs the parameter domains are taken to cover about $\pm$ 2 standard deviations of the corresponding amplitudes, i.e. the interval [-10,10] for ϑ_2, [-6,6] for ϑ_3, [-3,3] for ϑ_4 and [-2,2] for ϑ_5. The discretization steps are set to $\delta\vartheta_1$=1, $\delta\vartheta_2$=2.5, $\delta\vartheta_3$=2, $\delta\vartheta_4$=1.5 and $\delta\vartheta_5$=1. With these relatively large step sizes the computational burden for covering the 5-dimensional parameter space remains within limits, but the resulting discretization errors become large. To reduce ambiguity only 1/4 of these errors is considered for peak association, corresponding to 25% of the above step sizes. This is equivalent to subsampling the search space by partially covering the influence area about each discrete model state (25% in the direction of each EOF). An additional observation error of 10 msec is used for all peaks. The reference peak, used for the adjustment of arrival times, was chosen to be the first clear arrival peak. Hence, this particular peak had to be tracked for the whole experiment duration.

4.2. Relative-time inversion results

The oceanographic results obtained from the relative-time matched-peak inversion approach for the section K11-K12 are described first. The output of the matched-peak approach for each reception consists of a number of equally probable combinations of EOF amplitudes. From this population the mean value and variance (and thus the rms error) for each EOF amplitude can be calculated. Simultaneously with the solution for the EOF amplitudes an estimate of the differential clock drift can be obtained on the basis of eq. (9) for each reception. The results for the clock-drift are presented in the next section, in connection with the second-order clock drift corrections.

The mean amplitudes resulting from the sequence of daily receptions were further smoothed in time by applying a 5-day running average. Then the vertical sound-speed distributions were reconstructed by superposing the basic reference profile and the EOFs multiplied by their respective amplitudes. In the following the obtained sound-speed profiles were translated into potential temperature, using an empirical conversion relation. This relation had been deduced from hydrographic data collected in the Labrador Sea during the 1990s, neglecting the influence of salinity variations on sound speed; for the salinity effect an additional error was estimated and taken into account. Finally, the temperature profiles were vertically averaged to obtain layer mean values; in this analysis averages over for the upper 1300 m of the water column are presented.

In Figure 5 the evolution of the range- and depth-averaged potential temperatures for the section K11-K12 is shown, as obtained from the relative-time matched-peak inversion. The time series spans the 2nd year's deployment period from August 1997 until July 1998, represented by the horizontal axis in terms of yeardays of 1997. The line-connected dots represent the mean temperatures obtained from the tomography data whereas the shaded area indicates the rms inversion errors, the latter being equal to the square root of the temperature variance resulting from the population of model states obtained through the matched-peak approach for each reception, also taking into account their uncertainty in the conversion relation. A clear seasonal cycle can be seen in the temperature evolution, defined by warming until the end of

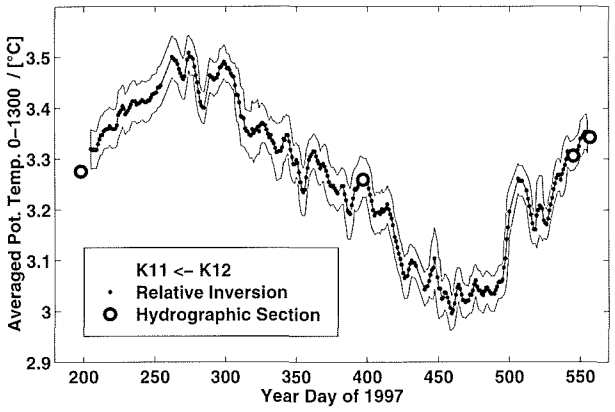

Figure 5. Temporal evolution of depth-averaged potential temperature in the layer 0-1300 m along the section K11-K12 from **relative**-time matched-peak inversions. The inversion results are marked with line-connected dots whereas the shaded area indicates the rms inversion errors. The open circles represent independent hydrographic observations.

September 1997, cooling which is mainly controlled by atmospheric forcing lasting until the end of March 1998 when minimum temperatures are reached, and warming starting again in mid April 1998.

The four open circles in Figure 5. represent the range- and depth-averaged temperatures along K11-K12 over the 0-1300-m layer calculated from independent hydrographic data. These data are from oceanographic surveys conducted along the line K11-K12 four times during the one-year period analyzed here. The first hydrographic measurement was used to correct the *absolute* travel times for an unknown offset in the mean distance between source and receiver. Nevertheless, in case of *relative-time* inversions this correction is of no relevance. No further adjustment neither of the travel times nor of the temperature curve has been made. Hence, all hydrographic observations have to be regarded as independent measurements. They match the relative-time inversion results surprisingly well, lying well within the inversion error tube in all four cases. Thus, they support the validity of the relative-time inversion results with respect to their oceanographic relevance. A comparison to absolute-time inversions follows after the application of differential clock drift corrections to travel-time data, as described in the next section.

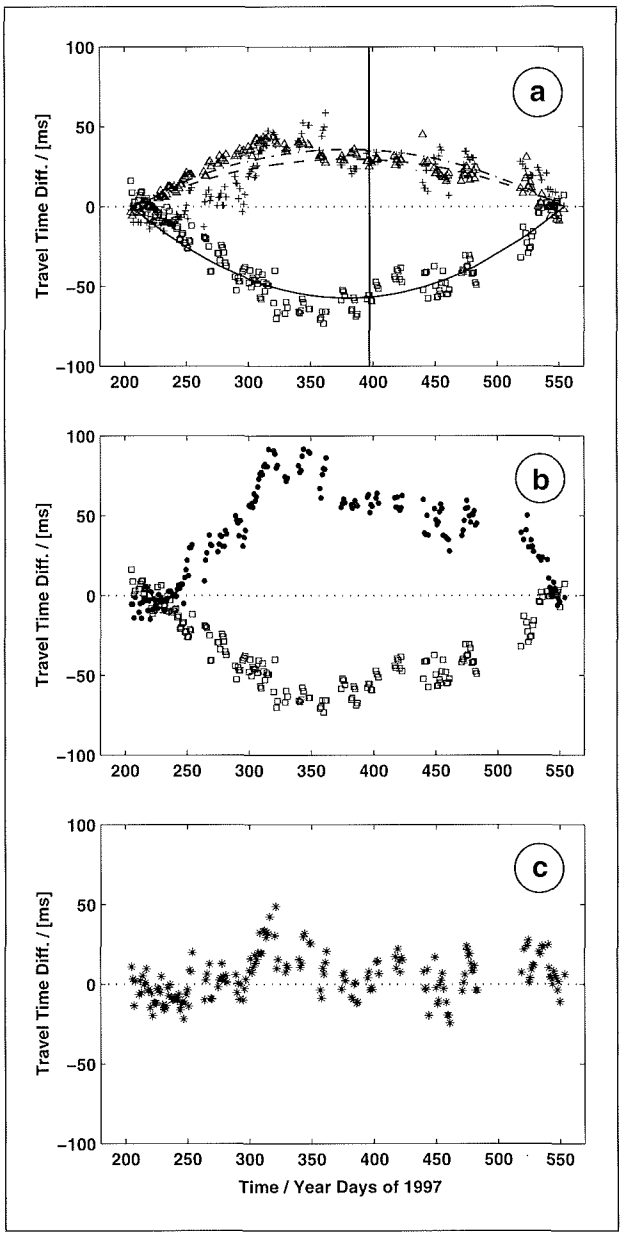

Figure 6. Differential clock-drift estimates, (a) for sections K11-K12 (squares), K11-K17 (crosses) and K12-K17 (triangles). Parabolic fits are denoted by solid, dashed and dash-dotted lines, respectively. Vertical line indicates time of hydrographic section. (b) Sum of clock-drift estimates for sections K11-K17 and K12-K17 (heavy dots) and estimates for K11-K12 (squares). (c) Sum of clock-drift estimates for all three sections.

4.3. Differential clock drift results

In the relative-time analysis clock-drift estimates are obtained simultaneously with the estimated model states (EOF amplitudes). In the matched-peak approach using a reference peak each discrete model state associated with a particular reception results in a value for the time shift $\delta\hat{t}$ on the basis of eq. (9). Thus, a population of equally probable time shifts corresponds to the matched-peak population of model states. The average time shift is considered as an estimate for the differential clock drift. "Differential" means that it is the estimated difference between the clock drifts of the transmitting and receiving instrument.

In Figure 6a the estimated differential clock drifts for the section K11-K12 (squares) are shown as obtained from the relative-time matched-peak inversions, simultaneously with the previous oceanographic results. On the same figure also the estimated clock drifts for K11-K17 (crosses) and K12-K17 (triangles) are shown. The estimates for K11-K17 were obtained in a similar manner from relative-time matched-peak inversions. For the section K12-K17, since reciprocal receptions (from quasi simultaneous two-way transmissions) were available, the differential clock drifts were estimated directly from reciprocal travel-time differences. This method

was preferred, since it delivers more accurate and smooth clock-drift results than the relative-time inversions.

The temporal evolution of clock drifts for all three sections clearly shows a parabolic behaviour reaching a maximum deviation from the linear (end-point) clock drift correction, of the order of -60 ms for K11-K12, 30 ms for K11-K17 and 40 ms for K12-K17, in the middle of the experiment. These estimates suggest that a second-order clock drift component (as observed in the Thetis 2 experiment as well [3]) is of significant importance. To derive corrections for the second-order clock drift components, a parabola was fitted to the estimated time series along each section; the maximum deviations of these parabolas are -57 ms, 30 ms and 37 ms for the sections K11-K12, K11-K17 and K12-K17, respectively. Each parabola was forced to zero at the beginning and end of the experiment; this is justified by the already applied end-point calibration (linear clock drift correction).

As a first consistency check of the estimated clock drifts the sum of the differential clock drifts for K11-K17 and K12-K17 is plotted in Figure 6b (heavy dots) against the differential clock drifts for K11-K12 (squares). In the absence of currents, the two quantities must have the same value but opposite sign [2]. Apart from a deviation of the K11-K17 and K12-K17 cumulative drift from the parabolic shape between yeardays 300 and 350, both temporal evolutions show a clear symmetry about zero. One reason for the observed deviation could be a strong oceanic current event, setting off travel times.

An equivalent check is to consider the circular integral of the individual clock drifts in the closed triangle K11-K17-K12-K11, which is equivalent to taking the sum of the drifts shown in Figure 6b. This sum should equal zero. Figure 6c shows the circular sum of estimated clock drifts results over the triangle. The concentration of the distribution about zero (except for the already mentioned period between yearday 300 and 360) underlines the consistency of the clock-drift estimates along the three sections.

A further test to confirm the estimated magnitude of the parabolic clock drift can be made using sound-speed data from the already mentioned hydrographic survey along K11-K12 around yearday 397 (cf. Figure 5), close to the middle of the one-year period, where the estimated deviation from the linear clock-drift is largest. Figure 7a shows the averaged acoustic arrival pattern (heavy line) recorded at K11 from K12 over the period of the hydrographic survey, with travel times resulting after the purely linear (end-point) clock drift correction. The light vertical lines on that figure represent *raytrace* K11-K12 predictions of the arrival times, for the first three groups of ray arrivals, using the range sound-speed profile from the hydrographic survey.

A comparison of those ray predictions with the first 9 observed clear peak arrivals (marked by dots in Figure 7a) reveals an offset in the observations of about 50 ms towards shorter travel times, which is attributed to the differential non-linear clock drift. The individual differences between predictions and observations are plotted against travel time in Figure 7b. It displays a distribution of time offsets about a mean value of 52 ms (dashed line). The corresponding value

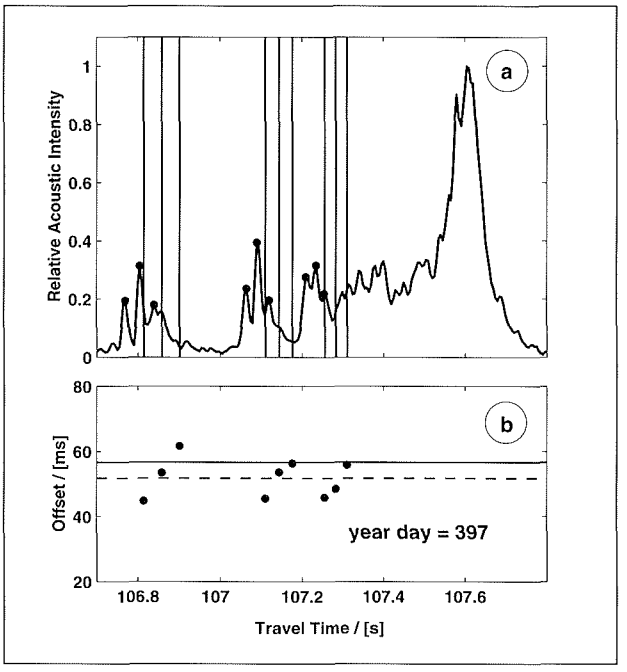

Figure 7. (a) Acoustic arrival pattern (heavy line) as recorded at K11 from K12 on yearday 397 and ray predictions (vertical lines) based on hydrographic data available at that time. The first 9 observed peak arrivals are marked by dots. (b) Differences between predicted and observed arrival times (heavy dots). The dashed line denotes the mean difference, while the solid line is the offset estimate from the K11-K12 parabolic fit of Figure 6a on yearday 397.

from the parabolic fit to the inversion-estimated differential clock drift between K11 and K12 is 57 ms (intersection between vertical line on yearday 397 and K11-K12 parabola in Figure 6a). The two values are close to each other and offer an additional confirmation for the accuracy of the clock-drift estimates obtained from the relative-time matched-peak inversion approach.

4.4. Absolute-time inversion results

Figure 8 shows the evolution of the range- and depth-averaged potential temperatures from the surface down to 1300 m for the section K11-K12, as obtained from absolute-time matched-peak inversions. The travel-time data used for these inversions were first corrected using the second-order correction (parabolic fit to the estimated clock drifts), shown in Figure 6a (solid line). As in Figure 5 the dots (connected by lines) and the shaded area represent the mean temperatures and the rms inversion errors, respectively, obtained from the (clock drift corrected) tomography data, whereas the four open circles denote temperatures obtained from independent hydrographic measurements.

Since the first hydrographic measurement (about yearday 198) was used to correct the absolute travel times for an unknown offset in the mean distance between source and receiver, the observed agreement of the first hydrographic point in Figure 8 with the inversion results is by construction. The other three hydrographic measurements, however, can be regarded as independent measurements, i.e. they can be

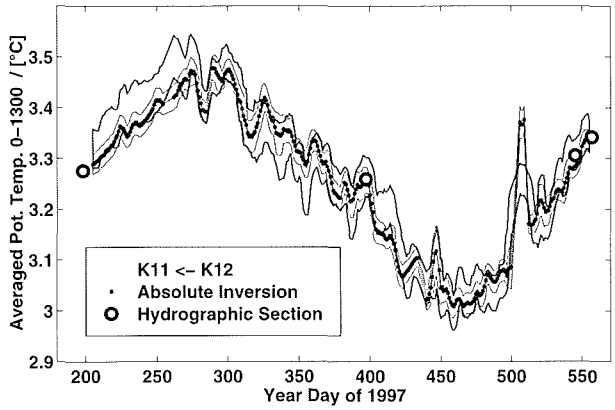

Figure 8. Temporal evolution of depth-averaged potential temperature in the layer 0-1300 m along the section K11-K12 from **absolute**-time matched-peak inversions, after second-order clock drift corrections were applied. The inversion results are marked with line-connected dots whereas the shaded area indicates the rms inversion errors. The heavy solid lines indicate the error tube from the **relative**-time inversions. The open circles represent independent hydrographic observations, as in Figure 5.

used for validation of the inversion results. All three match very well with the inversion results, i.e. they lie within the error tubes and nearly coincide with the mean temperature estimates (dots).

On Figure 8 also the error tube corresponding to the rms errors of the relative-time inversions is shown (heavy solid line) for comparison, taken from Figure 5. It is seen that the absolute-time inversion errors have about half the size of the relative-time inversion errors. This is due to the fact that the absolute arrival times contain more information than the relative ones and this leads to reduction of the inversion errors.

Furthermore, the two error tubes are overlapping well except for two short periods around yeardays 260 and 510. The deviation during the first period is due to the differences, observed in Figure 6a, between the estimated differential clock drifts for K11-K12 and the corresponding parabolic fit, which is constrained to zero at the beginning and at the end of the one-year experiment period (see previous section). Assuming that the clock drift indeed has a slow and smooth time evolution, the explanation for the deviation has to be a current signal, projected on the line connecting K11 and K12.

For the second period the observed peak in temperature (also seen in in travel-time, cf. Figure 4a) could be caused by an oceanic eddy, which passed the section near mooring K11 during this period. This is supported by independant local measurements at K11 which show a strong deep-reaching temperature increase at that time. In the travel-time data (Figure 4a) at the same time (i.e. at about day 510) a shrinking of the arrival time patterns and a displacement of about 50 ms is seen. If the displacement had been caused by current anomaly (along the line connecting K12 and K11, directed towards K11) a magnitude of about 0.7 m/s on average over the whole section would be necessary. This is more than expected for this area.

A similar displacement could also be caused by a temperature increase of about 0.2 °C, or by a combination of a current and a temperature anomaly with smaller amplitudes. One would need reciprocal transmissions to separate these two effects, but those are not available on this section. Since the local observations at mooring K11 show a deep-reaching warming of sufficient amplitude (down to about 800 m depth) we attributed the observed travel-time displacement to the barotropic (vertically constant temperature increase) compontent of the signal. By definition a displacment of the overall travel-time pattern can not be reproduced by relative-time inversions since these account only for a shrinking (or stretching) effect on travel-time patterns. We thus believe that this unusually deep anomaly is the reason why the temperature jump is only partially present in the time series resulting from the relative-time inversions. In contrast the absolute-time inversions account for both effects, yielding a temperature increase of larger amplitude.

5. Conclusions and discussion

In this work a relative-time matched-peak approach was applied to travel-time data from the Labrador Sea acoustic tomography experiment, in order to invert for the sound-speed field and simultaneously solve for an unknown travel-time offset. This approach was motivated by the suspicion, that for the clocks used in the tomographic transceivers a parabolic time drift of significant magnitude could be present (residual after linear correction by end-point calibration), which has to be determined and corrected for. The temporal evolution of the estimated differential clock drifts for the treated sections K11-K12, K11-K17 and K12-K17 clearly reveals a parabolic behaviour reaching maximum deviation from the linear correction of the order of 50 ms.

The consistency of the differential clock drift results – with respect to the three treated sections – could be shown by integrating the drifts around the triangle (described by the sections) yielding a close distribution about zero at almost any time of the experiment. Furthermore, a comparison of the estimated magnitude of the parabolic clock drift was made with respect to raytrace travel-time predictions based on sound-speed data from a hydrographic survey along K11-K12. That confirmed the representativeness of the results obtained from the relative-time matched-peak inversion approach for the time of that particular survey.

From the relative-time inversions oceanographic information in terms of vertically averaged temperatures, as deduced from the measured sound-speed field, were compared to independent hydrographic observations, yielding a satisfactory match, in all cases within the inversion errors. This underlines, that even with an unknown constant travel-time offset meaningful oceanographic results can be obtained using relative-time matched-peak inversions. A second-order clock-drift correction was obtained by fitting a parabola to the resulting clock-drift estimates. By applying this smooth correction to the travel-time data and performing absolute-time matched-peak inversions oceanographic results were

obtained that are in excellent agreement with the available independent observations. For future ocean acoustic tomography experiments an essential improvement of the quality of the internal time base of the instruments is expected, such that the described procedure to solve for unkown travel-time offsets will no longer be necessary.

The present analysis was based on ray-theoretic interpretation of the observed arrival patterns. In this connection it used the first 3-5 groups (triplets) of ray arrivals covering in most cases the largest part of the observed signals in the time domain. The later part of the receptions is difficult to treat in a ray-theoretic context and even though its variability is large it was not used. Normal modes and modal arrivals would be more suited for that part. Such an approach was followed in the Greenland-Sea experiment by using 90-m long vertical receiving arrays and applying spatial mode filtering to identify and track low-order modal arrivals [14]. However, in the Labrador-sea experiment the used receiving arrays are only 6-m long and mode filtering cannot be applied.

In this connection, it was considered to use at least the final cutoff of each arrival pattern, where the acoustic energy drops from a near maximum level to the noise level. This cutoff is easy to detect in the observed data and could be used to enhance the information content of deep ray arrivals, since in the present subpolar environment it probes the near-surface layers. Nevertheless, propagation studies showed a very high sensitivity of the last part of the arrival pattern and thus of the cutoff shape and cutoff time on the depth of the surface mixed layer [13]. As a result, the definition and modelling of the cutoff becomes unclear. In the light of these findings the final cutoff was not used for the inversions. The results obtained using the early arrivals confirm that these arrivals have sufficient information content for the 0–1300 m layer, even in their relative travel times.

Up to the time of writing a 4-year long time-series of ocean acoustic tomography data has been collected from the central Labrador Sea and the tomography measurements are ongoing. In the present work one year of these data was presented and analyzed. Future work will focus on the systematic analysis of the multi-year time series of data and on the oceanographic interpretation of seasonal and interannual variations with an emphasis on the large-scale integral effects of open ocean deep convection in the Labrador Sea. It was illustrated here that for the correct analysis of the tomography data the problem of the time offsets caused by non-linear clock drifts has to be addressed. Apart from other possible applications in connection to unknown travel-time offset, the used method of relative-time matched-peak inversions turned out to be an appropriate tool in this context.

References

[1] J. Marshall, F. Dobson, K. Moore, P. Rhines, M. Visbeck, E. d'Asaro, K. Bumke, S. Chang, R. Davis, K. Fisher, R. Garwood, P. Guest, R. Harcourt, C. Herbaut, T. Holt, J. Lazier, S. Legg, J. McWilliams, R. Pickart, M. Prater, I. Renfrew, F. Schott, U. Send, W. Smethie: The labrador sea deep convection experiment. Bull. Am. Met. Soc. **79** (1998) 2033–2058.

[2] W. H. Munk, P. F. Worcester, C. Wunsch: Ocean acoustic tomography. Cambridge U.P., New York, 1995.

[3] Thetis-2 Group: A pilot tomography system for monitoring the western Mediterranean basin. – In: Final Report. U. Send (ed.). EU MAST-2 project CT91-0006, March 1996.

[4] W. H. Munk, C. Wunsch: Ocean acoustic tomography: A scheme for large scale monitoring. Deep-Sea Res. **26A** (1979) 123–161.

[5] The Ocean Tomography Group: A demonstration of ocean acoustic tomography. Nature **299** (1982) 121–125.

[6] U. Send: Peak tracking by simultaneous inversion: Toward a one-step acoustic tomography analysis. J. Atm. Ocean. Techn. **13** (1996) 1116–1122.

[7] E. K. Skarsoulis, U. Send: One-step analysis of non-linear traveltime data in ocean acoustic tomography. J. Atmos. Oceanic Technology **17** (2000) 240–254.

[8] E. K. Skarsoulis: A matched-peak inversion approach for ocean acoustic travel-time tomography. J. Acoust. Soc. Am. **107** (2000) 1324–1332.

[9] R. A. Clarke, J.-C. Gascard: The formation of labrador sea water. Part I: Large-scale processes. J. Phys. Oceanogr. **13** (1983) 1764–1778.

[10] R. C. Spindel: Signal processing in ocean tomography. – In: Adaptive Methods in Underwater Acoustics. H. G. Urban (ed.). Reidel, Dordrecht, 1985.

[11] B. D. Cornuelle: Simulation of acoustic tomography array performance with untracked or drifting sources and receivers. J. Geophys. Res. **90** (1985) 9079–9088.

[12] E. K. Skarsoulis.: Multi-section matched-peak tomographic inversion with a moving transceiver. J. Acoust. Soc. Am. (2001) (in print).

[13] P. J. Sutton, P. F. Worcester, G. Masters, B. D. Cornuelle, , J. F. Lynch: Ocean mixed layers and acoustic pulse propagation in the Greenland Sea. J. Acoust. Soc. Am. **94** (1993) 1517–1526.

[14] P. J. Sutton, W. M. L. Morawitz, B. D. Cornuelle, G. Masters, , P. F. Worcester: Incorporation of acoustic normal mode data into tomographic inversions in the Greenland Sea. J. Geophys. Res. **99** (1994) 12487–12502.